國立臺灣大學「台大工程」學刊　第九十一期　民國九十三年六月　第 3–14 頁
Bulletin of the College of Engineering, N.T.U., No. 91, June 2004, pp. 3–14



# *MECHANICAL AND OPTICAL PROPERTIES OF InAs/GaAs SELF-ASSEMBLED QUANTUM DOTS*

# 砷化銦／砷化鎵自聚式量子點之機械與光學特性

林 資 榕[*]　郭 茂 坤[**]　廖 柏 亭[†]　洪 國 彬[*]

*Tzy-Rong Lin*　*Mao-Kuen Kuo*　*Bo-Ting Liao*　*Kuo-Pin Hung*

[*]博士生　[**]教授　[†]碩士班研究生
國立台灣大學應用力學研究所

[*] Ph.D. candidate　[**] Professor　[†] Graduate student
Institute of Applied Mechanics, National Taiwan University, Taipei, Taiwan 10617, R.O.C.

**摘　要**

本文旨在介紹自聚式量子點的特性、製程與應用，並以砷化銦／砷化鎵 (InAs/GaAs) 為基礎的自聚式量子點為例，分析其機械及光學特性。文中首先以線彈性力學理論，配合有限元素法套裝軟體，估算量子點內因異質材料間的晶格不匹配所引致的應變場分佈；再將此應變場效應，經由變形勢能，加入於薛丁格方程式中，而同樣以有限元素法分析，藉以評估應變效應對於導電帶、價電帶的特徵能量與電子、電洞機率密度函數分佈之影響，進而得到能帶間的電子躍遷能量與發光波長。由模擬結果得知，電子躍遷能量隨著量子點尺寸的增大而減小，亦即發光波長隨著量子點的增大而變長，此結果與文獻上的現象十分吻合。

**關鍵詞：** 自聚式量子點、應變場、有限元素法、薛丁格方程式。

**Abstract**

This article reviews the properties, growth mechanics, and applications of self-assembled quantum dots. A model based on theory of linear elasticity is developed to analyze the strain field induced by lattice-mismatch between quantum dot and substrate. The induced strain field is then incorporated, with the aid of the Pikus-Bir Hamiltonian and Luttinger-Kohn formalism, into the three-dimensional steady-state effective mass Schrödinger equation. Both the strain field and the solutions of the Schrödinger equations are solved numerically by using of a commercial finite element package. The energy levels as well as the wave functions of both conduction and valence bands of quantum dots are calculated. Finally energies of interband optical transitions are then obtained in numerical experiments. Numerical results show that the transition energy decreases with increasing of the dot size. This phenomenon agrees well with the previous results reported by others.

**Keywords**: self-assembled quantum dot, strain field, finite element method (FEM), schrödinger equation.

## 1. INTRODUCTION

One of the significant features of semiconductors is the energy gap which separates the conduction and valence energy bands. For instance, the color of light emitted by semiconductor materials is determined by the width of the energy gap. In semiconductors of macroscopic sizes, *i.e.*, bulk semiconductors, the widths of energy gaps are fixed parameters controlled by the semiconductors' identities.

On the other hand, in the cases of nanometer-sized semiconductors, with sizes around 10-100 nanometers, the situations change. It has been demonstrated that this range of the geometrical sizes of semiconductors is comparable with the spatial extents of the electronic wave functions. As results of the geometrical constraints, electrons will "sense" the presence of the geometrical boundaries of semiconductors and will respond to change accordingly by adjusting their energy. This phenomenon is known as the quantum confined

effect.

If one should define quantum dot exactly, it certainly has to be set out from the point of view of quantum mechanics. Since electrons have wave-particle duality, the property of electron waves depends on its Fermi-wavelength. In general, the wavelength of the electron is smaller than the size of the bulk material but comparable or even larger than the one of nano-scaled material. Therefore, the quantum confined effect is obvious. Usually, the nano-scaled materials have better acoustic, optic, electric, and thermal properties.

A quantum well is, in fact, a potential well which is very small in size. The "well" is like a box in which electrons would be trapped, in much the same way that light is trapped between mirrors. By making layers of different semiconductor materials, it is then possible to make a particular layer acts as a trap for electrons. It can take one more step further, by making a thin "wire", but not a layer, of the preferred semiconductor. These trapped electrons are then in two-dimensional quantum confinement (called quantum wire).

Quantum dots (QDs) are solid-state structures made of heterogeneous semiconductors or metals being capable of confining a countable, small numbers of electrons into a small space. The confinement of electrons is achieved by setting some insulating materials around a central, well conducting region. The densities of states for cases of bulk semiconductors, quantum wells, quantum wires and quantum dots are quite different as shown schematically in Fig. 1. Quantum dots have also been called artificial atoms.

Rapid developments on semiconductor technologies, especially various epitaxy techniques for preparing molecular layers of materials and lithography techniques for fabricating densely packed electrical circuits, have resulted in new possibilities for a creation of artificially ultra-small physical systems, say of sizes of couple nm, with controlled properties. In this unique situation, the manipulation of materials, however, meets with limitations imposed on small systems by quantum mechanics. Description of extremely small systems taken from macroscopic physics is irrelevant, as regards both optoelectronic properties and mechanical behavior. In this article, the size of QD is around 10's nm, hence the macroscopic viewpoint might still be feasible.

One of the most important factors driving the current active researches in quantum effect is the rapidly expanding on semiconductor band-gap engineering capability [1] offered by modern epitaxy, such as molecular beam epitaxy (MBE) and metallorganic chemical vapor deposition (MOCVD). MBE is a vacuum deposition technique carried out in an ultrahigh vacuum environment. It is a versatile technique for growing thin epitaxial structures made of metals, semiconductors and insulators.

MBE growth is carried out under conditions far from thermodynamic equilibrium, and it is governed mainly by the kinetics of the surface processes occurring when the impinging beams interact with the outermost atomic layers of the substrate crystal. MBE has a unique advantage over all other epitaxial growth techniques in significantly precise control on the beam fluxes and growth conditions.

In the cases of heteroepitaxial growth, one of the most important growth modes is so-called Stranski-Krastanow (SK) growth mode. The formation of Stranski-Krastanow islands is closely related to an epitaxial misfit and the accumulation of elastic strain energy in the epilayer. Strain relaxation takes place

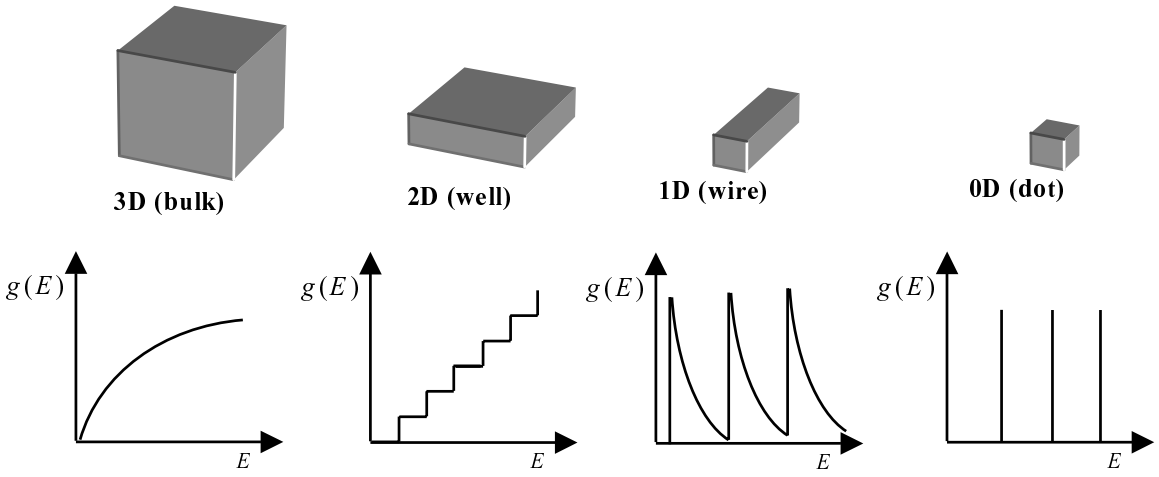


**Fig. 1 Densities of states as functions of energies in systems with different numbers of spatial dimensions: 3D, bulk material; 2D, quantum well; 1D, quantum wire; 0D, quantum dot**

through the rearrangement of the deposited material when 3D islands are formed. The formation of 3D islands changes completely the strain situation, which will then affect the optoelectronic properties of the quantum dots.

Quantum dots formed in the Stranski-Krastanow mode are called self-assembled dots. The small sizes of the self-assembled quantum dots, the homogeneity of their shapes and sizes in a macroscopic sample, the perfect crystal structure without edge defects, as well as the convenient growth process, without the need for any precise deposition of electrodes or etching, are among their greatest advantages, which stimulate hopes regarding their future application in electronics and optoelectronics, *e.g.*, quantum dot infrared detectors [3,4], quantum dot lasers [5,6] and quantum dot memory devices [7,8].

# 2. CONTINUUM AND QUANTUM MODELS

In this article, the analysis of the strained semiconductor nanostructures, self-assembled quantum dots (SAQDs), are divided into three parts. First, a linear elastic finite element calculation is performed to determine the strain distribution in and around SAQD nanostructures. Second, the carrier confinement potential in SAQD is modified by the strain distribution. The deformation potential theory is used to estimate the strain-induced potential superimposed to the energy bands of SAQD. Third, a steady-state three-dimensional Schrödinger equation is solved numerically to obtain the energy levels and wave function spectra in the SAQD. Finally, the energy of interband optical transitions is obtained in the numerical experiments.

## 2.1 Continuum Model

The strain fields inside and in the neighborhood of SAQD strongly affect the electronic properties, and hence the optoelectronic properties, in vicinity of the dots [9,10]. For the optoelectronic properties in III-V semiconductors (such as the materials are InAs and GaAs), there are two predominated strain effects, namely, changes of the conduction band level and the valence band level. The conduction band is only affected by the hydrostatic strain, often referred to as the dilatation or trace of the strain tensor. The valence level can change both with hydrostatic and biaxial strains. In addition, for zinc blende material structures, deviatoric strains give rise to piezoelectrically induced electric fields [11].

To understand the strain effects on optoelectronic properties of QD nanostructures, it is necessary to determine the elastic strain field in the quantum dots and surrounding matrix. There have been various methods in three different main categories: (1) Analytical continuum method [12~14], (2) Continuum finite element method (FEM) [15~18], and (3) Atomistic modeling [19~21]. Analytical continuum method leads to integral expressions for the elastic fields which can be integrated in closed forms for some simplest inclusion shapes, *e.g.*, cylindrical or spherical quantum dots. On the other hand, the interactions between the quantum dot and the surrounding material might have not been fully encountered. FEM is a very versatile and effective numerical method, which have capabilities to easily accommodate various theories and model on QD nanostructures to different levels. Atomistic models might be more reasonable to model systems in nano-scale provided that accurate interatomic potentials are available. Moreover, it requires a huge computing capacity to model quantum dots and the surrounding matrix. In the following sections, we first brief analytical continuum method and continuum finite element method for the QD problems, respectively. Then continuum finite element method will be used to study the SAQD nanostructures for the optoelectronic properties.

### 2.1.1 Analytical Continuum Method

Analytical continuum methods for calculating the strain and stress distributions attributed to a uniformly strained inclusion were originally developed by Eshelby [22]. From viewpoint of Eshelby's result, a quantum dot can be regarded as an inclusion embedded in an infinite matrix. Due to different lattice constants of the quantum dot and the matrix, the inclusion can be considered as initially strained to accommodate the mismatch in lattice constants. For general cases, having closed forms expression on analytical solutions of stress and strain distributions are not possible, except for some simple geometric shapes such as cubic, cylindrical, spherical, etc. Analytical solutions of the strain field for a buried pyramidal QD structure, including a truncated pyramidal quantum dot and a surrounding matrix, were presented by Pearson [23].

The problem of an initially uniformly strained QD of arbitrary shape embedded in an infinite isotropic medium can be solved analytically by theory of inclusion, under the simplification that both the QD and the matrix have the same elastic moduli. Based on previous works [24,25], a set of vectors has been chosen such that the divergence of each vector gave the Green's function for the stress component $\sigma_{ij}$. First, six vectors are defined as follows,

$$\begin{aligned}
\mathbf{A}_{xx}(x,y,z) &= \Lambda x\,\hat{i} \\
\mathbf{A}_{xz}(x,y,z) &= -\Lambda x\,\hat{k} \\
\mathbf{A}_{yy}(x,y,z) &= \Lambda y\,\hat{j} \\
\mathbf{A}_{xy}(x,y,z) &= -\Lambda y\,\hat{i} \\
\mathbf{A}_{zz}(x,y,z) &= \Lambda z\,\hat{k} \\
\mathbf{A}_{yz}(x,y,z) &= -\Lambda z\,\hat{j}
\end{aligned} \tag{1}$$

where

$$\Lambda = \varepsilon_0\, E/[4\pi(1-\nu)(x^2+y^2+z^2)^{3/2}]$$

and $\nu$ and $E$ are the Poisson ratio and the Young's modulus, respectively, of the QD and matrix. The misfit strain, $\varepsilon_0$, of the quantum dot is taken with respect to the surrounding matrix; and the quantum dot is assumed to be initially strained by $\varepsilon_0$ in all three directions, namely $x$-, $y$-, $z$-directions. This initial strain is taken as negative for dots, since it is under compression.

The vectors in Eq. (1) are chosen so that $\nabla\cdot\mathbf{A}$ leads to the Green's function stress components $\sigma^{sph}$ corresponding to a spherical point inclusion. Moreover, the above expressions for $\mathbf{A}$ is not unique because other choices of vectors $\mathbf{A}$ can also yield the Green's function stress components $\sigma^{sph}$ when taking divergence. For an arbitrary QD shape, the resultant integral to determine the stress $\sigma$ at the point $(x, y, z)$ is

$$\begin{aligned}
&\sigma_{ij}(x_1, x_2, x_3) \\
&= \int_V \left[\nabla\cdot\mathbf{A}(x_1-x_1^0, x_2-x_2^0, x_3-x_3^0)\right] \mathrm{d}V(x_1^0, x_2^0, x_3^0) \\
&= \int_V \sigma^{sph}(x_1-x_1^0, x_2-x_2^0, x_3-x_3^0)\ \mathrm{d}V(x_1^0, x_2^0, x_3^0) \\
&= \frac{\varepsilon_0 \mathrm{E}}{4\pi(1-\nu)} \int_V \frac{\delta_{ij}r'^2 - 3x_i'x_j'}{r'^5}\ \mathrm{d}V(x_1^0, x_2^0, x_3^0)
\end{aligned} \tag{2}$$

where $x_i^0$ means points inside $V$, the volume of the quantum dot, and $x_i' = x_i - x_i^0$, $\delta_{ij}$ is the Kronecker delta and $r'^2 = x_i'x_i'$. The summation convention on repeated index has been assumed through this article. Therefore, the solution for a spherical inclusion can be used as a Green's function for the three-dimensional problem. This Green's function was then integrated over the volume of the QD which gives rise to the stress field of the QD.

The analytical stress field of a pyramid QD and a truncated pyramid QD, as illustrated in Fig. 2, can be obtained by evaluating Eq. (2) and expressing in closed form, especially with the aid of any available algebraic software package. The volume of a rectangular-base,

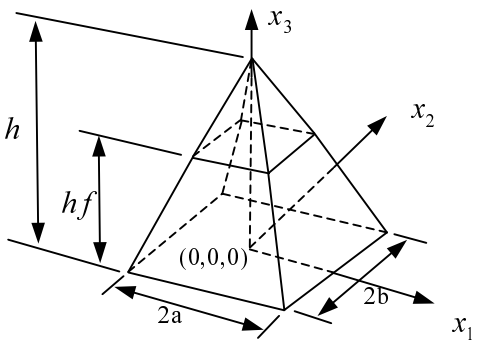


**Fig. 2 The geometries of the pyramid and truncated pyramid QD**

truncated pyramid QD is defined by,

$$\begin{aligned}
-a\left(1-\frac{x_3^0}{h}\right) &\le x_1^0 \le a\left(1-\frac{x_3^0}{h}\right) \\
-b\left(1-\frac{x_3^0}{h}\right) &\le x_2^0 \le b\left(1-\frac{x_3^0}{h}\right) \\
0 &\le x_3^0 \le hf
\end{aligned} \tag{3}$$

where $h$ means the height of the pyramid QD in the absence of truncation and $f$ represents the degree of truncation, $0 \le f \le 1$. Once each stress component $\sigma_{ij}$ has been calculated, substituting $\sigma_{ij}$ into the Hooke's law, of isotropic elastic solids, gives the strain fields:

$$\varepsilon_{ij} = \frac{1}{E}\left[(1+\nu)\sigma_{ij} - \delta_{ij}\nu\sigma_{kk}\right] \tag{4}$$

Equations (2) and (4) enable us to calculate the stress and the strain fields for a single uniformly strained pyramid QD of arbitrary truncation embedded in an infinite medium. For systems containing more than one QD, the principle of superposition of linear problems allows the stresses (strains) at a point to be determined by simply summing the stresses (strain) field of each single QD in the arrays.

Notice that in this analysis, both quantum dots and matrix are assumed as isotropic elastic solids with the same elastic moduli, though it is far away from the reality. Moreover, the QD is assumed to be deformed initially only without any further elastic deformation. The full interaction between QD and the matrix may have not been taken into account properly. Besides, the matrix is assumed to be of unbounded extent; hence effects of free surfaces have not yet been included in this formulation.

### 2.1.2 Continuum Finite Element Method

Another important category of methods on

computing the stress and strain fields induced by QD is the continuum finite element method (FEM). FEM gives only the numerical results for quantum dots. On the other hand, it works even for rather complex geometries, and provides a complete picture of the strain distribution of a three-dimensional model. In addition, assumptions of isotropic as well as same elastic moduli as in previous methods are not needed here. Furthermore, with the improvement of computer technology, it becomes much easier even to handle heavy tasks, especially 3D (three dimension) problems with FEM. Benabbas [26] and Muralidharan [16] gave a 2D (two dimension) axisymmetric model to analyze the strain distribution inside and in the neighborhood of QD. A 3D model for strain field was presented in [27].

Notice that the mismatch of lattice constants will induce further elastic deformation in the whole nanostructure system, namely, in both the substrate and the quantum dot island. In other words, the lattice mismatch will not be the only strain in the quantum dot island. In these works, the lattice mismatch between dot and substrate is simulated under the framework of the theory of thermo-elasticity. For these calculations, both QD and substrate are assigned to have corresponding hypothetical coefficients of thermal expansion, in order to produce a desired misfit across the interface matching the initial strain from lattice-mismatched. For example, growing InAs on (001) GaAs substrate by molecular beam epitaxy (MBE) results in pyramid-like islands (dots) [28~30]. The lattice mismatch between InAs and GaAs is about 6.7%. The initial strain field induced by lattice mismatch can then be simulated by setting the hypothetical coefficient of thermal expansion of the DQ and the substrate to be as $0.067°K^{-1}$and 0, respectively, with a raised temperature by 1°K.

In the numerical experiments of this article, a buried pyramidal InAs/GaAs SAQD nanostructure, as depicted schematically in Fig. 3, is considered. The InAs dot is self-assembled under certain conditions during heteroepitaxy on (001) GaAs substrates on which a thin wetting layer is grown first, followed by coherent island formation. The dot is subsequently covered by additional substrate materials. Epitaxially grown semiconductor heterostructures, such as SAQDs, often consist of several materials with different lattice constants. The mismatch of lattice constants gives rise to the strain field in a QD nanostructure, which will then affect the optoelectronic properties of the quantum dots. The model based on the linear elasticity theory will be developed to evaluate the strain distribution in and around the InAs/GaAs SAQD nanostructure.

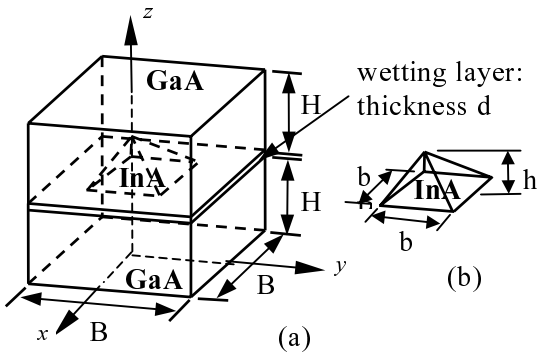


**Fig. 3 Schematics of (a) the buried InAs/GaAs QD nanostructure : B = 30nm, H = 30nm, d = 0.5nm, and (b) the island (InAs dot) b = pyramid width, h = pyramid height**

In-plane (the base plane of QD) lattice mismatch parameter is usually defined as

$$(\varepsilon_0)_{xx} = (\varepsilon_0)_{yy} = \frac{a_s - a_d}{a_d} \tag{5}$$

where $a_s$ and $a_d$ are the lattice constants of the substrate material and the QD, respectively. Notice that the mismatch of lattice constants will induce further elastic deformation in the whole nanostructure system, namely, in both the substrate and the QD island. In other words, the lattice mismatch parameter defined in Eq. (5) will not be the only strain in the quantum dot island, it will instead be treated as in-plane initial strain in the latter finite element analysis. On the other hand, the out-of-plane initial strain has never yet been as conclusive as its in-plane counterparts. In this article, the out-of-plane initial strain is set to zero such that the initial strain tensor is given as

$$\boldsymbol{\varepsilon}_0 = \begin{bmatrix} (\varepsilon_0)_{xx} & 0 & 0 \\ 0 & (\varepsilon_0)_{yy} & 0 \\ 0 & 0 & 0 \end{bmatrix} \tag{6}$$

Based on the theory of linear elasticity, the stress-strain relation of anisotropic solids with initial strains can be written as:

$$\boldsymbol{\tau}_{ij} = C_{ijkl}[\boldsymbol{\varepsilon}_{kl} - (\boldsymbol{\varepsilon}_0)_{kl}] \qquad i, j, k, l = x, y, z \tag{7}$$

where $\tau_{ij}$ and $\varepsilon_{kl}$ are the stress and total strain tensors, respectively. $C_{ijkl}$ is the elastic moduli tensor, and $(\varepsilon_0)_{kl}$ is the initial strain tensor defined in Eq. (6). Here both GaAs and InAs are treated as cubic materials with 3 independent elastic moduli each. A list of material properties used, including lattice constants and elastic moduli, is summarized in Table 1.

**Table 1 Material properties**

| Mechanical property | $a_0$ (nm) | $C_{11}$ (GPa) | $C_{12}$ (GPa) | $C_{44}$ (GPa) |
|---|---|---|---|---|
| GaAs | 0.565 | 118.79 | 53.76 | 59.4 |
| InAs | 0.605 | 83.29 | 45.26 | 39.6 |

| Deformation potential | $a_c$ (eV) | $a_v$ (eV) | $b$ (eV) |
|---|---|---|---|
| GaAs | −7.17 | 1.16 | −1.7 |
| InAs | −5.08 | 1 | −1.8 |

| Effective mass[a] | $m_e(m_0)$ | $M_{lh,xy}(m_0)$ | $M_{hh,z}(m_0)$ |
|---|---|---|---|
| GaAs | 0.067 | 0.115 | 0.333 |
| InAs | 0.023 | 0.035 | 0.263 |

[a]From Luttinger-Kohn parameters $\gamma_1, \gamma_2, \gamma_3$

The linear elasticity boundary value problem, arising from the mismatch in lattice constants between the wetting layer, QD island and substrate materials, is analyzed, here, using a commercial finite element package FEMLAB. Appropriate boundary conditions are needed in the analysis: all the nodes of the outer surfaces parallel to the $x$- and $y$-outer surfaces are fixed in the normal displacement due to periodic symmetric argument. The bottom outer surface is fixed against displacement in $z$-direction to avoid rigid body shift; whiles the upper surface is kept traction free. The displacement compatibility across the interface of island/ substrate is satisfied automatically in the finite element formulation with displacement field as unknowns.

It is worthwhile to point out that the wetting layer and QD island grew on the substrate and embedded within the capping layer, as depicted in Fig. 3. In the conventional analysis, the capping layer is assumed to be deformed together with QD and substrate. On the other hand, in fact, in the fabrication process, the capping layer is deposited after the QD has been deformed to compensate the mismatch of lattice constants. Hence the capping layer should have never been experienced the deformation of QD at all, in fabrication process. To take this sequence of fabrication process into account, in this article, the capping layer is added into the nanostructure system only after the strain analysis of quantum dot and substrate has been completed, and is assumed to be unstrained thereafter. After the strain field has been calculated, the capping layer is added when solving the Schrödinger equation. This is equivalent to assume that the strain distribution in the QD does not to affect the capping layer.

It is also of interest to point out that QDs are grown in a large array instead of a single dot actually. In a finite element model, it is easy to consider a single dot or a regular array of dots. However, the strain distribution within a disordered array of dots will still be impractical, if not impossible, to be obtained by using finite element methods. FEM is rather computationally intense compared to analytic solutions. To obtain results to certain accuracy, the grid size must be kept small enough; however, as the grid size is reduced, the demand on computational memory and time increases rapidly. The choice of the grid size depends on the accuracy required and computer capacity and time available.

## 2.2 Quantum Model

The band structure is determined by considering the difference in band gap energies of the heterostructure constituent materials. A part of band gap difference is taken up by a conduction band offset, and a portion results in a valence band offset, as shown in Fig. 4, for the cases that QD and substrate are taken as InAs and GaAs, respectively.

The strain effects will induce an extra potential field, $V_{\text{strain}}$. For the strained QD nanostructure, the confinement potential can be written as a sum of energy offsets of the conduction band (or valence band), $V_{\text{band}}$, and the strain-induced potential, $V_{\text{strain}}$, as

$$V(\vec{r}) = V_{\text{band}}(\vec{r}) + V_{\text{strain}}(\vec{r}) \tag{8}$$

The strain contribution to the potential is determined via deformation potential theory, modified by the strain tensor $\varepsilon_{ij}$. It may then affect the energy band structure for the QD, altering further optoelectronic properties in the devices.

Here, Pikus-Bir Hamiltonian [9,10] together with the computed strain field from above-mentioned strain field calculations (section 2.1.2) are used to determine strain-induced potentials in QD. It is known that the conduction band level will be only affected by the hydrostatic strain [11], and the strain-induced potential for the conduction band can be expressed as [9]

$$V^c_{\text{strain}} = a_c\,(\varepsilon_{xx} + \varepsilon_{yy} + \varepsilon_{zz}) \tag{9}$$

On the other hand, the valence level can be changed with not only hydrostatic strain but also biaxial strain. The strain-induced potential for the valence band can then be written as [10]

$$V_{\text{strain}}^{v} = a_v(\varepsilon_{xx}+\varepsilon_{yy}+\varepsilon_{zz}) - \frac{b}{2}(\varepsilon_{xx}+\varepsilon_{yy}-2\varepsilon_{zz}) \quad (10)$$

where $a_c$ is the deformation potential constant of conduction band; while $a_v$ and $b$ denote the deformation potential constants of valence band. The data of these three constants for InAs and GaAs are summarized in Table 1. The strain-induced potentials are computed according to Eqs. (9) and (10) and are superimposed to energy band. In our cases, all other potential energy contributions, such as piezoelectric potential energy, are expected to be small and are neglected in the calculations.

The behavior of individual carrier in QD nanostructures is governed by the three-dimensional steady state Schrödinger equation as:

$$\left[-\frac{\hbar^2}{2}\nabla_{\vec{r}}\left(\frac{1}{m^*}\right)\nabla_{\vec{r}} + V(\vec{r})\right]\psi_n(\vec{r}) = E_n\,\psi_n(\vec{r}) \quad (11)$$

Equation (11) is solved numerically again, in this article, by means of a commercial finite element method package, FEMLAB, to obtain energy levels and the wave functions in a QD nanostructure. The boundary conditions on the quantum dot/substrate interfaces are

$$\begin{cases} \psi_d = \psi_s \\ \dfrac{1}{m^*_{d_{n_i}}}\dfrac{d\psi_d}{dn} = \dfrac{1}{m^*_{s_{n_i}}}\dfrac{d\psi_s}{dn} \end{cases} \quad (12)$$

where subscripts $d$ and $s$ denote the QD and substrate regions, respectively, $n$ denotes the normal directions of interfaces, and a carrier effective mass is taken along the normal directions of interfaces. In addition, at the top of the capping layer, bottom of the substrate, and their outer surfaces, the wave function is set to zero.

Based on the computed energy and wave function distributions, the energy of interband optical transitions can readily be obtained. The optical conductivity features peaks at particular wavelengths of light that are more strongly absorbed; these wavelengths in turn can be expected to be the strongest emission wavelengths.

## 2.3 Numerical Results

The geometry of an embedded InAs/GaAs QD nanostructure considered here is depicted in Fig. 4; the

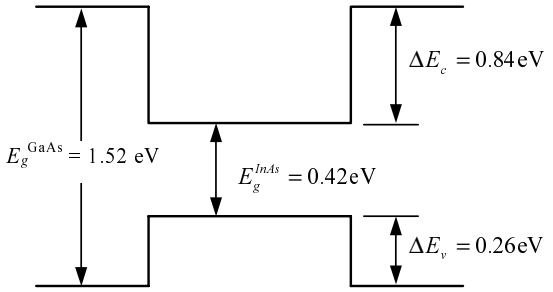


**Fig. 4 Initial energy band of the unstrained InAs/GaAs heterostructure used for quantum dot calculations**

**Table 2 Dimensions of the QD nanostructures**

| Structure | I | II | III | IV | V |
|---|---|---|---|---|---|
| width b (nm) | 12 | 12 | 12 | 16 | 20 |
| height h (nm) | 3 | 4 | 6 | 6 | 6 |

InAs QD is assumed to be as pyramidal shape with square-based of width b. Sizes of QD used in the numerical experiments of the article are listed in Table 2. The semiconductor materials are treated as anisotropy during the strain analysis. As mentioned in section 2.1.2, since the capping layer does not experience the deformation of QD in the self-assembled process; in the stage of strain analysis, the QD heterostructure system is considered to consist of only quantum dot, wetting layer and substrate but not capping material. Once the strain analyses have been completed, the capping layer is then added into the system. The adding of capping material is only for the purpose of solving the Schrödinger equation to obtain the electronic structure of the nanostructure system.

In this model, the capping layer is consequently assumed to be unstrained. The model takes the sequence of fabrication process into account. It is equivalently to neglect the re-distribution of strain in

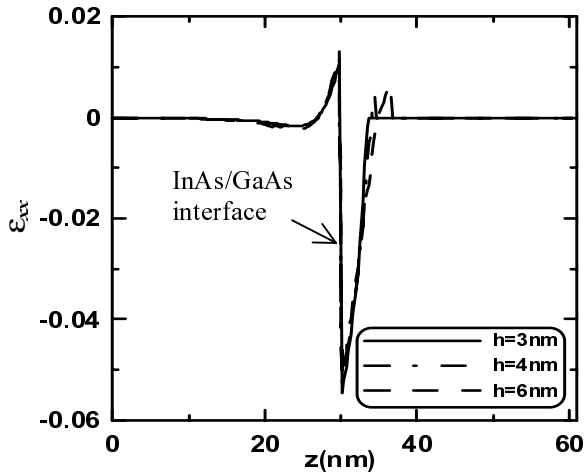


**Fig. 5 Strain components $\varepsilon_{xx}$ plotted along the $z$-axis for structure I, II, and III**

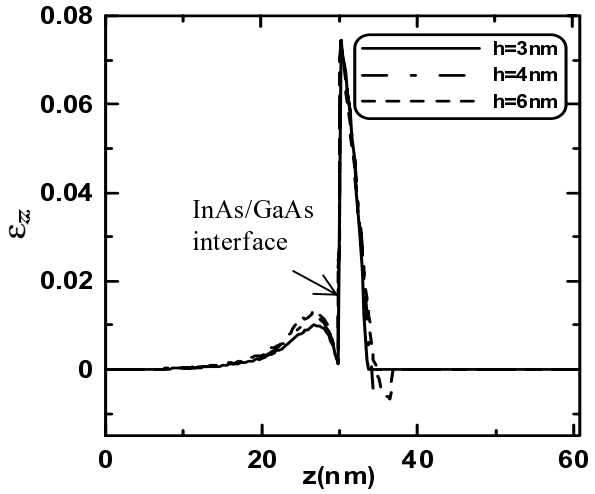


**Fig. 6 Strain components $\varepsilon_{zz}$ plotted along the $z$-axis for structure I, II, and III**

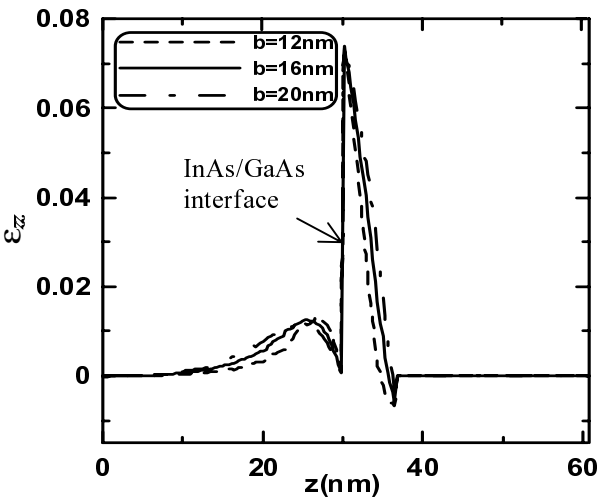


**Fig. 8 Strain components $\varepsilon_{zz}$ plotted along the $z$-axis for structure III, IV, and V**

the QD system during the depositing process of the capping layer, which is expected to be much small compared to the strain distribution in the QD and in the substrate material.

Strain components $\varepsilon_{xx}$ and $\varepsilon_{zz}$, are shown in Figs. 5 and 6, respectively, along $z$-axis in QD structures for the cases of width $b$ = 12nm with various heights ($h$ = 3, 4, and 6nm). These strain components show ample discontinuities across the interface of InAs wetting layer and the GaAs substrate (*i.e.* InAs/GaAs interface), as one would expect. Moreover, the strain field $\varepsilon_{xx}$ inside the QD is compressive while $\varepsilon_{zz}$ is tensile. These reflect the fact that the lattice constant of InAs is larger than that of GaAs. Similarly, strain components $\varepsilon_{xx}$ and $\varepsilon_{zz}$, are shown in Figs. 7 and 8, respectively, along $z$-axis in QD structures for the cases of height $h$ = 6nm with various widths ($b$ = 12, 16, and 20nm).

From Figs. 5 ~ 8, it is easily to conclude that strain

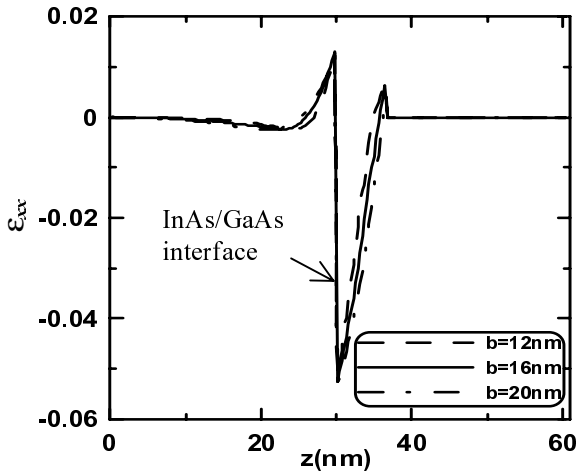


**Fig. 7 Strain components $\varepsilon_{xx}$ plotted along the $z$-axis for structure III, IV, and V**

fields are larger for larger QD size, as one would expect, since a larger QD can be viewed as a larger source of initial-strain field.

The calculated ground state energy level and corresponding transition energy in the QD nanostructure are summarized in Table 3. The transition energy is defined as the energy difference between the electron and the hole. The peak of experimental photoluminescence (PL) spectra is related to the transition energy. From the numerical results in Table 3, it is seen that the energy of interband optical transition becomes smaller as the island size increasing. This phenomenon agrees well with the previous experimental photoluminescence data [31].

Probability density function profiles, given by square of wave functions, namely $|\psi|^2$, for the ground state energy levels in the QD nanostructures, are shown in Fig. 9. Subfigures 9(a) and 9(b) are the probability density function profiles corresponding to electron and hole, respectively, energy levels for the structure I ($h$ = 3nm). Similarly, subfigures 9(c) and 9(d) are for the case of the structure III, namely $h$ = 6nm. It is easily to see that, from Fig. 9, the probability density function distributions are confined almost entirely to the island region. Moreover, the probability density function distributions of electrons appear to be spherical symmetry within the whole island, subfigures 9(a) and 9(c). On the other hand, the probability density function distributions of hole are likely to be more confined in the bottom of the island, subfigures 9(b) and 9(d).

Similarly, Fig. 10 shows the probability density function profiles of the first excited energy levels of the electron and the hole. Again, subfigures 10(a) and 10(b) correspond to the electron and to the hole, respectively, for the case of $h$ = 3nm; while subfigures

**Table 3 Ground state energy level and the transition energy (eV)**

| | Electron energy | Hole energy | Transition energy |
|---|---|---|---|
| Structure I | 1.302 | 0.203 | 1.099 |
| Structure II | 1.239 | 0.216 | 1.023 |
| Structure III | 1.150 | 0.229 | 0.921 |
| Structure IV | 1.113 | 0.268 | 0.845 |
| Structure V | 1.095 | 0.295 | 0.800 |

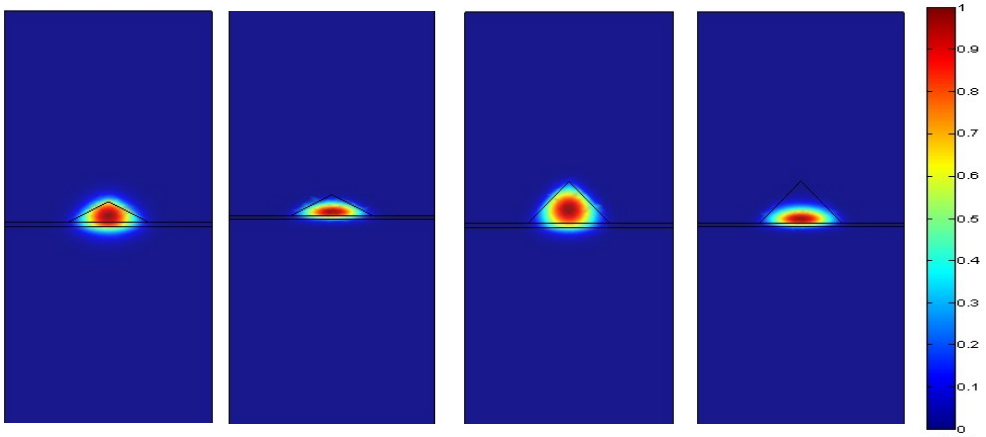


**Fig. 9 Probability density function profiles for energy levels of the ground state in the *yz*-plane through the dot center. For QD structure I: (a) electron energy; (b) hole energy. For QD structure III: (c) electron energy; (d) hole energy**

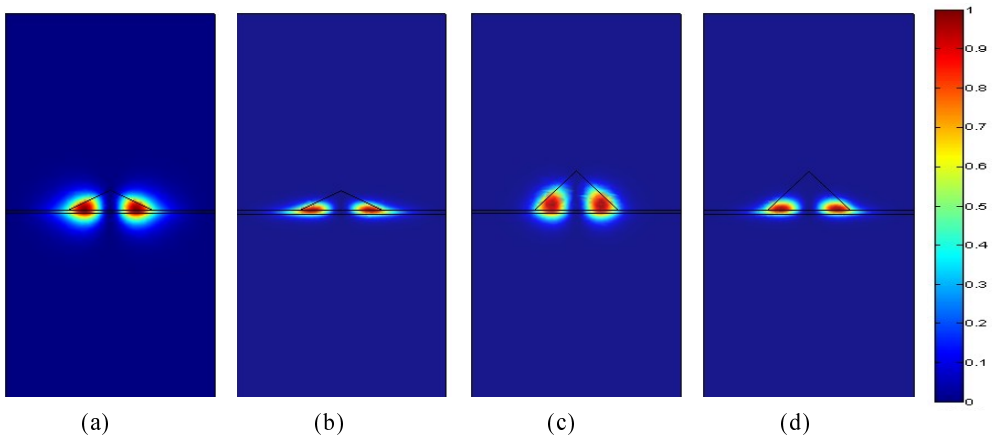


**Fig. 10 Probability density function profiles for energy levels of the first excited in the *yz*-plane through the dot center. For QD structure I: (a) electron energy; (b) hole energy. For QD structure III: (c) electron energy; (d) hole energy**

10(c) and 10(d) are for the case of $h$ = 6nm. Compared to probability density function distributions of the ground state, namely to the Fig. 9, the ones of first excited state are confined more at the corner of quantum dot.

The calculated transition energies range from 1.1 eV to 0.8 eV which correspond to 1128nm and 1550nm in the optical wavelength spectrum. This wavelength spectra spread in the infrared radiation.

## 3. CONCLUSIONS

In this article, a model has been presented for analyzing mechanical and optoelectronic coupling in the pyramidal InAs/GaAs SAQD nanostructure. The model is based on theory of linear elasticity and has taken the sequence of the fabrication process into account to analyze three-dimensional induced strain field by mismatch of lattice constants in quantum dots.

Further, the energy levels and wave function distributions in SAQD nanostructures have also been studied by solving the steady state three-dimensional effective mass Schrödinger equation. The effects of the strain-induced potential have been considered through Pikus-Bir Hamiltonian. Finally energies of interband optical transitions are obtained in numerical experiments.

In the article, the fact that transition energy decreases with increasing the quantum dot size has been revealed through numerical computation. This phenomenon agrees well with the previous results reported by others. The wavelengths of the optical transition energies in pyramidal InAs/GaAs SAQD nanostructures considered in the article range from 1128 nm to 1550 nm in the optical wavelength spectrum. The wavelength spectra will be mostly attractive in the applications of optical fiber communications. The InAs/GaAs SAQD nanostructures would have great potential in future optical applications.

## ACKNOWLEDGMENTS

This work is carried out in the course of research sponsored by the National Science Council of Taiwan under Grant No. NSC92-2212-E-002-072.

## REFERENCES

[1] S. S. Iyer, G. L. Patton, J. M. C. Strok, B. S. Meyerson and D. L. Harame, "Heterojunction bipolar transistors using Si-Ge Alloys," *IEEE Trans. Electron Devices*, 1989, p. 2043.

[2] E. Bauer and J. H. van der Merwe, "Structure and growth of crystalline superlattices: From monolayer to superlattice," *Phys. Rev. B*, Vol. 33, 1986, p. 3657.

[3] S. Maimon, E. Finkman, G. Bahir, S. E. Schacham, J. M. Garcia and P. M. Petroff, "Intersublevel transitions in inAs/GaAs quantum dots infrared photodetectors," *Appl. Phys. Lett.*, Vol. 73, 1998, p. 2003.

[4] J. L. Jiminez, L. R. C. Finseca, D. J. Brady, J. P. Leburton, D. E. Wohlert and K. Y. Cheng, "The quantum dot spectrometer," *Appl. Phys. Lett.*, Vol. 71, 1997, p. 3558.

[5] L. Harris, D. J. Mawbray, M. S. Skolnick, M. Hopkinson and G. Hill, "Emission spectra and mode structure of InAs/GaAs self-organized quantum dot lasers," *Appl. Phys. Lett.*, Vol. 73, 1998, p. 969.

[6] D. L. Huffaker, G. Park, Z. Zou, O. B. Shchekin and D. G. Deppe, "Discrete energy level separation and the threshold temperature dependence of quantum dot Lasers," *Appl. Phys. Lett.*, Vol. 73, 1998, p. 2564.

[7] J. J. Finley, M. Skalitz, M. Arzberger, A. Zrenner, G. Bohm and G. Abstreiter, "Electrical detection of qptically induced charge storage in Self-Assembled InAs quantum dots," *Appl. Phys. Lett.*, Vol. 73, 1998, p. 2618.

[8] Amlani, A. O. Orlov, G. L. Snider, C. S. Lent and G. Bernstein, "Demonstration of a Six-Dot quantum cellular automata system," *Appl. Phys. Lett.*, Vol. 72, 1998, p. 2179.

[9] G. E. Pikus and G. L. Bir, "Effects of deformation on the hole energy spectrum of gernasium and silicon," *Sov. Phys. Solid State*, Vol. 1, 1960, pp. 1502–1517.

[10] G. E. Pikus and G. L. Bir, *Symmetry and Strain-Induced Effects in Semiconductors*, Wiley New York, 1974.

[11] S. L. Chuang, *Physics of optoelectronic devices*, John Wiley & Sons, New York, 1995.

[12] V. A. Shchukin, D. Bimberg, V. G. Malyshkin and N. N. Ledentsov, "Vertical correlations and anticorrelations in multisheet arrays of two dimensional islands," *Phys. Rev., B*, Vol. 57, 1998, p. 12262.

[13] D. Andreev, J. R. Downes, D. A. Faux and E. P. O'Reilly, "Strain distributions in quantum dots of arbitrary shape," *J. Appl. Phys.*, Vol. 86, 1999, p. 297.

[14] G. S. Pearson and D. A. Faux, "Analytical solutions for strain in pyramidal quantum dots," *J. Appl. Phys.*, Vol. 88, 2000, p. 730.

[15] T. Benabbas, Y. Androussi and A. Lefebvre, "A finite element study of strain fields in vertically aligned inas islands in gaAs," *J. Appl. Phys.*, Vol. 86, 1999, p. 1945.

[16] G. Muralidharan, "Strains in InAs quantum dots embedded in GaAs: A finite element study," *Jpn. J. Appl. Phys.*, Vol. 39, 2000, L 658.

[17] H. T. Johnson, L. B. Freund, C. D. Akyüz and A. Zaslavsky, "Finite element analysis of strain effects on electronic and transport properties in quantum dots and wires," *J. Appl. Phys.*, Vol. 84, 1998, p. 3714.

[18] L.B. Freund and H.T. Johnson, "The influence of strain on confined electronic states in semi-conductor quantum structures," *J. Mech. Phys. Solids*, Vol. 38, 2001, p. 1045.

[19] M. Tadic, F. M. Peeters, K. L. Janssens, M. Korkusinski and P. Hawrylak, "Strain and band edges in single and coupled cylindrical inas/ gaas and inp/ingap self-assembled quantum dots," *J.*

*Appl. Phys.*, Vol. 92, 2002, p. 5819.

[20] C. Pryor, J. Kim, L. W. Wang, A. J. Williamson and A. Zunger, "Comparison of two methods for describing the strain profiles in quantum dots," *J. Appl. Phys.*, Vol. 83, 1998, p. 2548.

[21] M. E. Bachlechner, A. Omeltchenko, A. Nakano, R. K. Kalia, P. Vashishta, I. Ebbsjö, A. Madhukar and P. Messina, "Multimillion-Atom molecular dynamics simulation of atomic level stresses in Si(111)/Si3N4(0001) nanopixels," *Appl. Phys. Lett.*, Vol. 72, 1998, p. 1969.

[22] J. D. Eshelby, "The Determination of the Elastic Field of an Ellipsoidal Inclusion and Related Problems," *Proc. R. Soc. London*, Ser. A 241, 1957, pp. 376.

[23] G. S. Pearson and D. A. Faux, "Analytical solutions for strain in pyramidal quantum dots," *J. Appl. Phys.*Vol. 88, 2000, P. 730.

[24] D. A. Faux, J. R. Downes and E. P. O'Reilly, "A simple method for calculating strain distributions in quantum wire structures," *J. Appl. Phys.*, Vol. 80, 1996, p. 251.

[25] J. R. Downes, D. A. Faux and E. P. O'Reilly, "A simple method for calculating strain distributions in quantum dot structures," *J. Appl. Phys.*, Vol. 81, 1997, p. 6700.

[26] T. Benabbas, P. Francois, Y. Androussi and A. Lefebvre, "Stress relaxation in highly strained inas/gaas structures as studied by finite element analysis and transmission electron microscopy," *J. Appl. Phys.*, Vol. 80, 1996, p. 2763.

[27] G. R. Liu and S. S. Quek Jerry, "A finite element study of the stress and strain fields of inas quantum dots embedded in GaAs," *Semicond. Sci. Technol.*, Vol. 17, 2002, p. 630.

[28] M. Geiger, A. Bauknecht, F. Adler, H. Schweizer and F. Scholz, "Observation of the 2D-3D growth mode transition in the InAs/GaAs system," *J. Grys. Growth*, Vol. 170, 1997, p. 558.

[29] S. Ruvimov, P. Werner, K. Scheerschmidt, U. Gosele, J. Heydenrenich, U. Richter, N. N. Ledentsov, M. Grundmann, D. Bimberg, V. M. Ustinov, A. Y. Egorov, P. S. Kop'ev and Z. I. Alferov, "Structural characterization of (In,Ga) as quantum dots in a GaAs matrix," *Phys. Rev. B*, Vol. 51, 1995, p. 14766.

[30] D. Bimberg, M. Grundmann, N. N. Ledentsov, S. Ruvimov, P. Werner, U. Richter, J. Heydenrenich, V. M. Ustinov, P. S. Kop'ev and Z. I. Alferov, "Self-Organization processes in MBE-Grown quantum dot structures," *Thin Solid Films*, Vol. 267, 1995, p. 32.

[31] F. Heinrichsdorff, A. Krost, M. Grundmann, D. Bimberg, F. Bertram, J. Christen, A. Kosogov and P. Werner, "Self organization phenomena of InGaAs/GaAs quantum dots grown by metalorganic chemical vapour deposition," *J. Crys. Growth*, Vol. 170, 1997, p. 568.

**Tzy-Rong Lin** (林 資 榕) is currently a Ph.D. candidate of Applied Mechanics at the National Taiwan University, Taipei, Taiwan. His research is mainly in the area of mechanical and optoelectronic coupling in semiconductor nanostructures.

**Mao-Kuen Kuo (郭 茂 坤)** received his B.S. and M.S. degrees in civil engineering from National Taiwan University, Republic of China, in 1977 and 1979, respectively, and Ph.D. degree in civil engineering from Northwestern University, United States of America, in 1984.
Presently, he is a Professor in the Institute of Applied Mechanics, National Taiwan University. He joined the faculty of National Taiwan University in 1984. His research work is mainly on Elastodynamic Fracture Mechanics and Nondestructive Evaluation. He was a recipient of the 1987 Teaching Award sponsored by the Ministry of Education, Republic of China. He was also recipients of the 1987, 1988, 1989 and 2002 Teaching Award sponsored by the College of Engineering, National Taiwan University.

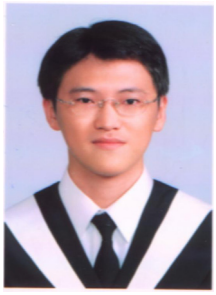

**Bo-Ting Liao (廖 柏 亭)** received the B.S. degree in mechanical engineering from the National Cheng Kung University, Tainan, in 2002. He now studies the M.S. degree in Institute of Applied Mechanics, National Taiwan University, Taipei, Taiwan. His research focuses on the mechanical and optoelectronic properties of nanostructures.

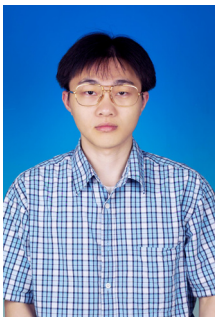

**Kuo-Pin Hung (洪 國 彬)** received the M.S. degree in Institute of Applied Mechanics at the National Taiwan University, Taipei, Taiwan in 2003. He is now a Ph.D. student in Institute of Applied Mechanics, National Taiwan University. His research is mainly on the piezoelectric mechanics and electronic properties of semiconductor.

收稿日期 93 年 5 月 10 日、修訂日期 93 年 5 月 23 日、接受日期 93 年 5 月 27 日
Manuscript received May 10, 2004, revised May 23, 2004, accepted May 27, 2004